Numerical Methods in Civil Engineering

The Particle Filter and Extended Kalman Filter methods for the structural system identification considering various uncertainties

Mehrdad Ebrahimi*, Reza Karami Mohamadi, Fatemeh Sharafi*****

ARTICLE INFO

Article history:
Received:
December 2019.
Revised:
January 2020.
Accepted:
February 2020.

Keywords:
System identification, Extended Kalman Filter, Particle Filter, FE model updating, modeling uncertainty.

Abstract:

Structural system identification using recursive methods has been a research direction of increasing interest in recent decades. The two prominent methods, including the Extended Kalman Filter (EKF) and the Particle Filter (PF), also known as the Sequential Monte Carlo (SMC), are advantageous in this field. In this study, the system identification of a shake table test of a 4-story steel structure subjected to the base excitation has been implemented using these methods by considering the modeling and material model uncertainties. Implementing the 2D and 3D modelings, using the "parallelogram" and "scissors" methods for the modeling of panel zones and that of the wall panels by two methods (using beam-column elements and equivalent diagonal strut elements), are the assumptions of this study. Using the parallelogram method has resulted in fewer errors in the 2D modeling while implementing different methods for simulation of wall panels has had no specific achievements. As illustrated in the results, more significant uncertainties were expected in systems with highly nonlinear behavior, since the equivalent linearization was used to estimate the system states in the EKF method. However, this method is less time-consuming and gives more accurate results in comparison with the PF method, in which a lrge number of samples are required for the system identification.

1. Introduction

Structural system identification using the earthquake-induced vibrations has drawn the attention of researchers and engineers in recent years. This method can be categorized into the model-based and non-model-based approaches. Model-based methods identify the state of the system using a structural model with geometrical and mechanical properties, while according to the non-model-based methods, the system's input and output have been employed for identification of the system state. Among model-based methods, despite the complications of the finite element (FE) model updating method, some advantages have been achieved [1-7].

** Ph. D. Candidate, Department of Civil Engineering, K.N. Toosi University of Technology, Tehran, Iran.*
*** Corresponding Author: Associate Professor, Department of Civil Engineering, K.N. Toosi University of Technology, Tehran, Iran.*
Email: rkarami@kntu.ac.ir
**** M.Sc. in Earthquake Engineering, Department of Civil Engineering, K.N. Toosi University of Technology, Tehran, Iran.*

According to this method, the differences between the recorded responses in the real structure and the FE model are minimized. As real-world structures have a nonlinear behavior under several excitations and even ambient vibrations, using the nonlinear FE model updating method has drawn much more attention from researchers [8-14]. Considering the
damage that occurred in the structure during the earthquake, this method can identify the damage type, location, intensity, and the structure's remaining life (service life). In fact, the method takes advantage of an optimization technique to determine different indices of the FE model so that the difference between the real structure and its simulation is minimized. Therefore, simulating the numerical FE model is an essential and challenging part of this method, demanding accurate modeling of components and material models with regard to different uncertainties.

Based on another classification, identification methods can be categorized into offline methods and online or recursive methods [15]. In online methods, the inputs and outputs of

the structure, recorded in each time step has been used for the model updating and modification of the errors. Unlike the online method, it seems impracticable to modify the errors during the data recording process in the offline methods, in which data recording continues until the last step.

Different recursive methods such as the recursive Least Square (RLS) [16-18], sequential Monte Carlo or particle filter (PF) [19-22], and Kalman Filter (KF) [23-26] have been used for the structural system identification. For the PF method, the posterior probability of the system's state is estimated by the generation of a considerable amount of weighted samples, using Monte Carlo methods. PF methods possess extended point-mass filters, in which particles have not uniformly distributed over the system's state, but concentrated in high probability areas, except for its major shortcoming concerning the large number of samples that increases the calculation time. On the contrary, although the KF method is less time-consuming, it is not an appropriate technique for nonlinear systems. To cope with this problem, the developed KF methods, such as the extended Kalman Filter (EKF), have been used for several decades, based on which problems have been solved by linearizing the system around the latest estimated state in a state-space format [27-30]. However, it is not useful in highly nonlinear systems [31].

Although these methods are widely used for the identification of structural systems, several complexities and uncertainties in the calibration of real structures such as model simplifications, inappropriate boundary conditions, and behavior of material models have continued to exist. In this study, the PF and EKF capabilities in the identification of a one-bay 4-story steel frame located on a shake table are investigated, considering the aforementioned uncertainties. For this purpose, five models are used including 1) 2D model with the panel zone effects using parallelogram modeling [32], 2) 2D model with the panel zone effects using scissor modeling [33], 3) 3D model without the panel zone effects, 4) 3D model without the panel zone effects by considering the interaction of the frame and perimeter walls using beam-column elements, 5) 3D model with the interaction of frame and perimeter walls using equivalent diagonal strut elements.

Concerning the 2D modeling, nonlinear behavior of beam-column elements and panel zones is represented using concentrated plasticity, while nonlinear behavior is represented by the distributed plasticity in the 3D modeling. For concentrated plasticity models, the nonlinear behavior of beams and columns is simulated using the Modified Ibarra Krawinkler (MIK) material model [34], and the panel zone effects are considered using the Krawinkler [35] and the Fielding and Huang models [36]. Furthermore, for 3D models, the Giuffre-Menegotto-Pinto (G-M-P) [37] model is assigned to beam-column fiber sections, as well as several material models used to display the behavior of wall panels. The acceleration responses of stories of the structure are utilized in the system identification as well.

This paper is organized as follows: First, the PF and EKF algorithms are briefly explained. Then, the structural properties are identified. Subsequently, the modeling and the material modeling details and characteristics are discussed. Finally, the methods are compared, and the conclusion is derived.

2. System equations, PF and EKF methods:

The dynamic equation governing the behavior of a nonlinear system with multiple degrees of freedom in the state-space format is given below:

$$\dot{x} = F(x(t), u(t)) + v_t \tag{1}$$

The system response is defined as:

$$y_k = G(x_k, u_k) + \eta_k \tag{2}$$

where x_k is system state at the time $= k\Delta t$; v(t) is the process noise with zero mean and the covariance matrix Q(t); y_k is the system output in $t = k\Delta t$, and η_k is the measurement noise with the covariance matrix $R_k(t)$. Equations (1) and (2) are defined in a discrete format by the following equations:

$$x_{k+1} = f(x_k, u_k) + v_k \tag{3}$$

$$y_k = g(x_k, u_k) + \eta_k \tag{4}$$

where v_k is the process noise with the covariance matrix Q_k.

To determine the system state x_k using recorded responses until time step k, ($y_{1:k}$), the posterior probability density function $p(x_k|y_{1:k})$ is required. Assuming that the prior probability density function $p(x_0)$, and the density function in the time step (k-1), are known, the probability density function, $p(x_k|y_{1:k-1})$ is calculated by equation (5):

$$p(x_k|y_{1:k-1}) = \int p(x_k|x_{k-1})p(x_{k-1}|y_{1:k-1})\, dx_{k-1} \tag{5}$$

The probabilistic model of the state evolution $p(x_k|\, x_{k-1})$, also known as the transitional density, is defined by equation (3). Hence, using the recorded measurements at the time k (y_k), the estimated state can be updated in the following way:

$$p(x_k|y_{1:k}) = p(x_k|y_k, y_{1:k-1}) = \frac{p(y_k|x_k)p(x_k|y_{1:k-1})}{p(y_k|y_{1:k-1})} \tag{6}$$

where $p(y_k|y_{1:k-1})$ depends on $p(y_k|x_k)$ function, determined by equation (4).

2.1. Particle filter

In the following section, the theorem of the particle filter, summarized by Arulampalam et al. [38], is briefly reviewed. The main concept of the particle filter method is based on a posterior probability density function (PDF), and the particles have been sampled to estimate the system's state. Each particle has a likelihood of weighting, assigned to it. The particle filtering computes the posterior density function using a set of particles, x_k^i in which i=1,2,…, N and their weights referred to as ω_k^i. To determine the importance of weights, importance sampling considered as a general technique to estimate the properties of a particular distribution is used, which is different from the one used for generating samples.

If samples are generated from a density B(x), which is similar to A(x), then it can be described as:

$$\forall x, A(x) > 0 \rightarrow B(x) > 0 \tag{7}$$

Then any integral of the form I= $\int A(x)dx$ is rewritten as:

$$I = \int \frac{A(x)}{B(x)} B(x)dx \tag{8}$$

A Monte Carlo estimate is then determined in order to draw N independent samples from B(x) to form the weighted sum:

$$I_N = \frac{1}{N}\sum_{i=1}^{N} w_k^i \delta(x_k - x_k^i) \tag{9}$$

where w_k^i equals to $\frac{A(x^i)}{B(x^i)}$ and $\delta(x)$ is the Dirac delta function. Consequently, the probability density function at the time step k is calculated as follows:

$$p(x_k|y_{1:k}) = \sum_{i=1}^{N} w_k^i \delta(x_k - x_k^i) \tag{10}$$

where $\omega_k^i \propto \frac{A(x_k^i|y_{1:k})}{B(x_k^i|y_{1:k})}$ and x_k^i involve N samples extracted from importance density function $B(x_k^i|y_{1:k})$ at time step k. It is to be noted that the sum of the weight values can be equal to unity since the values are normalized. The state space form ω_k^i, is estimated by the following recursive relation [39]:

$$\omega_k^i \propto \omega_{k-1}^i \frac{A(y_k|x_k^i)A(x_k^i|x_{k-1}^i)}{B(x_k^i|x_{k-1}^i, y_k)} \tag{11}$$

where $A(x_k^i|x_{k-1}^i)$ is the transitional density obtained from equation (3), and $A(y_k|x_k)$ is computed through using equation (4).

One of the main drawbacks of the particle filter algorithm is that, during a time step, a substantial weight value assigned to one particle and the updating of other particles containing small weight values and having insignificant effects on $A(x_k|y_{1:k})$, is time-consuming. As such, resampling, in which the particles with small weight values have been disregarded and substantial weight values of particles have been considered, can be applied in an attempt to solve this problem. Thus, the particles with large weight values become more effective, and their weight values are uniformly considered to be equal to 1/N. However, replacing the small weight values with large weight values in sequential time steps eradicates the variation of particles and induces uniform distribution. In this regard, some techniques, such as the crossover operator method, can be used in comparison to the technique used in the Genetic Algorithm [40]. Finally, as the particles tend to infinity, the system states tend to the average value. However, this increases the computational cost compared to the EKF calculations that consume less time.

Fig. 1 briefly represents the application of the particle filter algorithm. In the first step, the particles are selected using the importance density. In the second step, importance weights are extracted using likelihood functions. Then, inappropriate samples that have small weight values are resampled. Finally, the predicted probability density function is calculated by weighted particles.

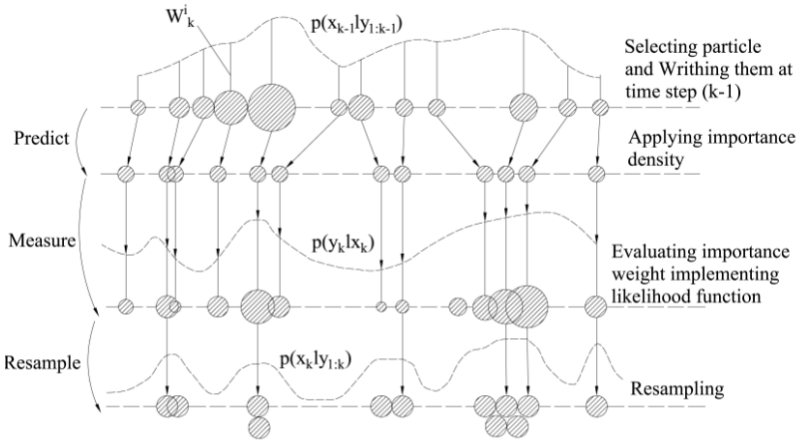

Fig. 1: Schematic representation of the particle filter (PF) algorithm [21].

2.2. Kalman Filter

The behavior of a nonlinear system in state-space format has been described in Equation (3). For linear systems, the Kalman Filter is used to estimate the system states (system parameters and responses) under the system inputs and noises in the state-space format. Hence, it is not useful for the estimation of nonlinear system states. Different methods for the estimation of nonlinear system states have been proposed in the literature, among which the EKF provides the advantages? by linearizing the system in the state-space format through the first-order Taylor series (a comprehensive review of the KF method for linear systems and EKF for nonlinear systems can be found in Ebrahimian et al. [41]). Then the equations of linear system states can be estimated and determined. Subsequently, the posterior estimate of the system in each step is considered as the center point of the linearization for the next step, which can be defined as follows:

$$x_{k+1} = \left[f_k(\hat{x}_k^+, u_k) + \left.\frac{\partial f_k(x,u_k)}{\partial x^T}\right|_{x=\hat{x}_k^+} (x_k - \hat{x}_k^+) + H.O.T \right] + v_k \rightarrow x_{k+1} \cong A_k x_k + \tilde{u}_k + v_k \quad (12)$$

where $\tilde{u}_k = f_k(\hat{x}_k^+, u_k) - A_k \hat{x}_k^+$ and $\mathrm{A_k} = \left.\frac{\partial \mathrm{f_k}}{\partial \mathrm{x^T}}\right|_{\mathrm{x}=\hat{\mathrm{x}}_\mathrm{k}^+}$.

Employing the first-order approximation and assuming $v_k = N(0, Q_k)$, where $N(\mu, C)$ is the normal distribution with a mean of μ and the covariance matrix of C, the prior estimate of the system state and the covariance matrix ($\hat{x}_{k+1}^-$ and $\hat{P}_{x,k+1}^-$) are obtained from the following equations:

$$\hat{x}_k^- = f_k(\hat{x}_k^+, u_k) \quad (13)$$

$$\hat{P}_{x,k+1}^- = A_k \hat{P}_x^+ A^T{}_k + Q_k \quad (14)$$

To perform a posteriori estimation of the system states and the covariance matrix ($\hat{x}_{k+1}^+$ and $\hat{P}_{x,k+1}^+$), the response matrix of the system must also be linearized around the latest estimated state. Hence, the following equation can be arranged as:

$$y_{k+1} = \left[g_{k+1}(\hat{x}_{k+1}^+, u_{k+1}) + \left.\frac{\partial g_{k+1}(x,u_{k+1})}{\partial x^T}\right|_{x=\hat{x}_{k+1}^-} (x_{k+1} - \hat{x}_{k+1}^-) + H.O.T \right] + \eta_{k+1} \rightarrow y_{k+1} \cong C_{k+1} x_{k+1} + \tilde{z}_{k+1} + \eta_{k+1} \quad (15)$$

Where $C_{\mathrm{k+1}} = \left.\frac{\partial \mathrm{g_{k+1}}}{\partial \mathrm{x^T}}\right|_{\mathrm{x}=\hat{\mathrm{x}}_{\mathrm{k+1}}^-}$ and $\tilde{z}_{k+1} = g_{k+1}(\hat{x}_{k+1}^-, u_{k+1}) - C_{k+1}\hat{x}_{k+1}^-$. Assuming that w and v are two independent Gaussian noises and $\eta_k = N(0, R_k)$, the linearized first-order estimate is defined as:

$$\hat{y}_{k+1}^- = g_{k+1}(\hat{x}_{k+1}^-, u_{k+1}) \quad (16)$$

$$\hat{P}_{xy,k+1}^- \cong \hat{P}_{x,k+1}^- C_{k+1}^T \hat{P}_{y,k+1}^- \cong C_{k+1} \hat{P}_{x,k+1}^- C_{k+1}^T + R_{k+1} \quad (17)$$

Where $\hat{y}_{k+1}^-$ is predicted system response and $\hat{P}_{xy,k+1}^-$ is the estimated cross-covariance matrix of the system state at the time step k+1. The Kalman Filter algorithm for the recursive nonlinear systems is summarized in Fig. 2, where $E[]$ is used to determine the expected values provided in parentheses.

In this study, the EKF method, in which the main objective is to determine the mean and variance of variables using inputs and outputs of the system, has been utilized to extract the parameters of the nonlinear system. Provided that the inputs and outputs of the nonlinear system are known, and the parameters of the material models of the system are assumed to be fixed, the EKF method can be used. According to this method, parameters are defined as random variables.

For this method, the system outputs are defined as:

$$y_{k+1} \cong h_{k+1}(\theta, u_{k+1}) + \eta_{k+1} \quad (18)$$

Where θ is a constant parameter vector, and h(.) describes the nonlinear system. To solve the equation, the parameters vectors are assumed to be randomly distributed and changed by the Gaussian Markov process. The state-space equation for the parameters and the system output is then defined as:

$$\theta_{k+1} = \theta_k + \gamma_k \quad (19)$$

$$y_{k+1} = h_{k+1}(\theta_{k+1}, u_{k+1}) + \eta_{k+1} \quad (20)$$

Equations (19) and (20) describe the state of linear systems, in which γ_k is assumed as a zero-mean Gaussian process. If the measurement noise of the system is assumed to be equal to the zero-mean Gaussian, the recursive EKF method can extract the mean value and the covariance of parameter vectors using previous equations, as well as the inputs and outputs of the system in each time step. Only, the equation of the system outputs must be linearized.

The mechanical properties of the test structure and the characteristics of the base excitations are noticed in the following sections. Furthermore, the FE models of the structure and the material models are explained, and then the application of the PF and EKF algorithms is described.

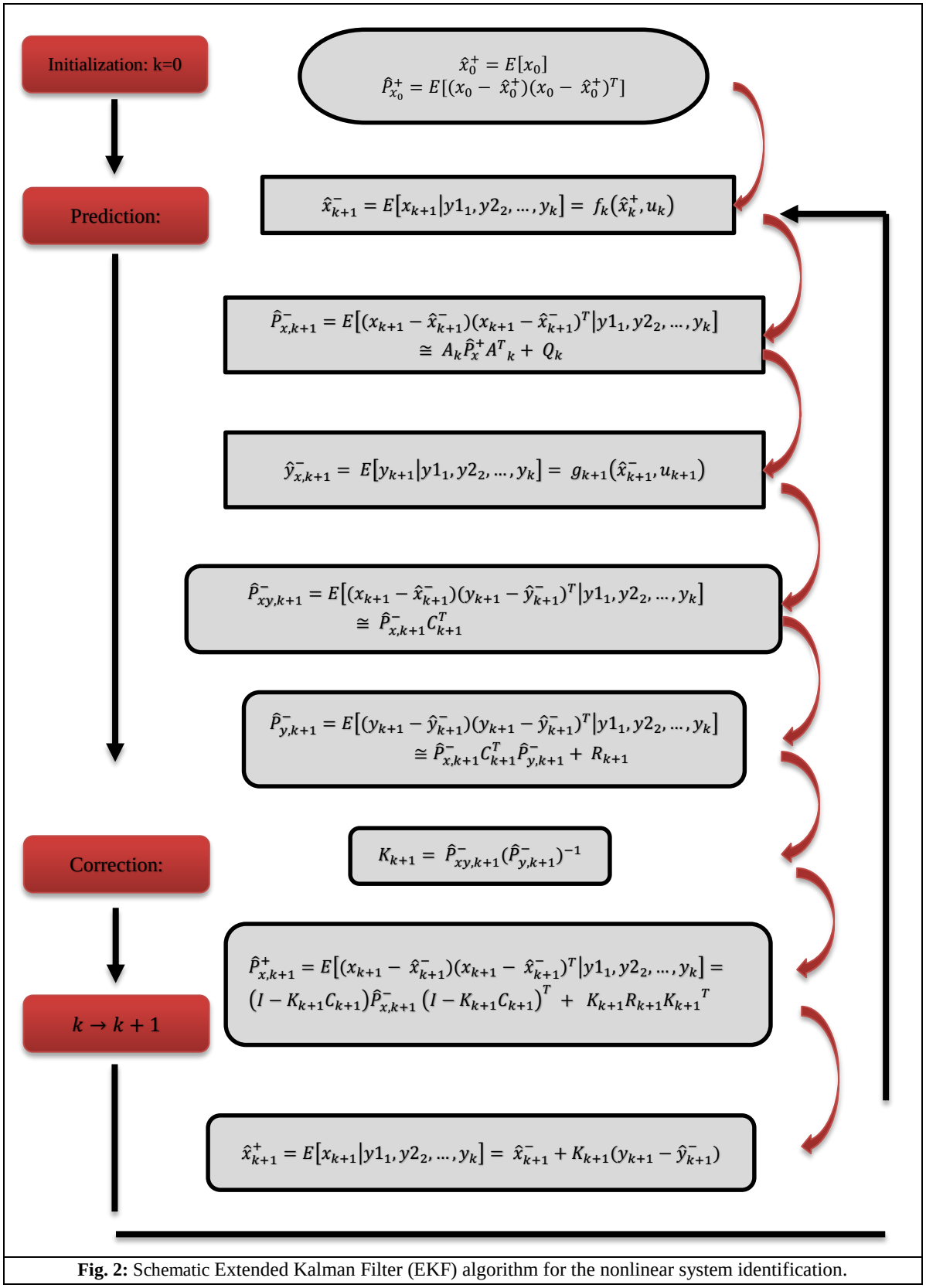

Fig. 2: Schematic Extended Kalman Filter (EKF) algorithm for the nonlinear system identification.

3. The test structure characteristics

To consider the uncertainties and errors in real structure modeling, a three-dimensional 4-story steel structure with two spans in one direction and one span in another direction, tested in the National Research Institute for Earth Science and Disaster Prevention (NIED) in 2007 is simulated (Fig. 3) [42]. As shown in Fig. 4, the structure has two spans of 5 meters in the Y-direction and one span of 6 meters in the X-direction, and the story heights are

3.875 m for the first story and 3.5 m for the remaining stories of the structure. Table 1 shows the beam and column sections of the structure. The beams are fabricated from the Japanese SN400B structural steel with the nominal yield strength of 235MP. The columns are designed as square hollow sections, having a nominal yield strength of 295 MP based on the Japanese BCR295 structural steel. The roof system consists of composite slabs with 175 mm concrete cover, which are connected to beams by shear studs. As such, a contribution between the slabs and beams is expected. On the other hand, as shown in Fig. 4, the structure is surrounded by Autoclaved Lightweight Concrete (ALC) panels in all directions, except for one peripheral frame in the Y-direction. Therefore, the interaction of panels and the structure is anticipated. In this study, the displacement and acceleration data of the structure on a shake table test, which have been recorded at a frequency of 100Hz, are used for the system identification.

Fig. 3: Full-scale 4-story steel structure after the completion of the NIED shaking table [42].

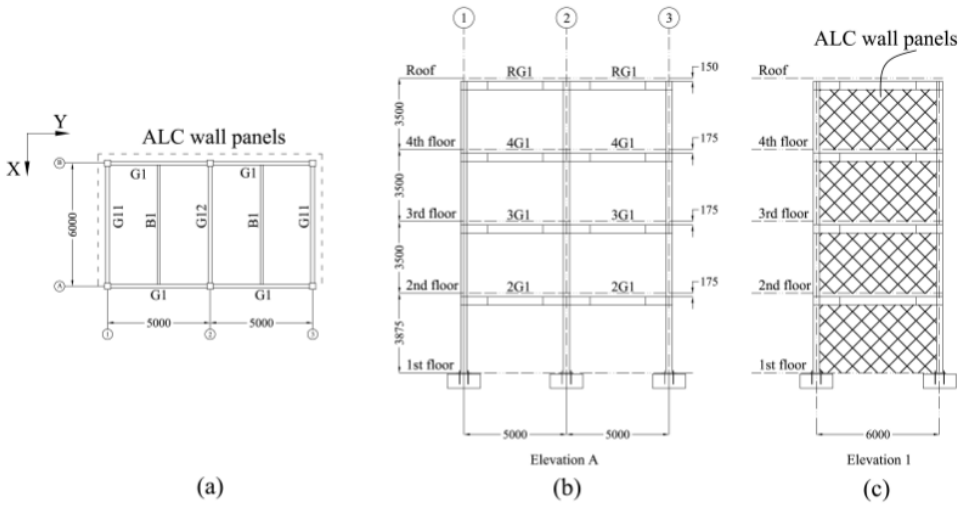

Fig. 4: Four-story prototype building: (a) plan view of a typical story, (b) Y-elevation, and (c) X-elevation (units: millimeters)

Table 1. Beam and column sections of the 4-story steel structure.

	Beam sections				Column sections
Floor	G1(SN400B)	G11(SN400B)	G12(SN400B)	Story	C1, C2
Roof	H346 × 174 × 6 × 9	H346 × 174 × 6 × 9	H346 × 174 × 6 × 9	4	HSS 300 × 9
4	H350 × 175 × 7 × 11	H350 × 175 × 7 × 11	H340 × 175 × 9 × 14	3	HSS 300 × 9
3	H396 × 199 × 7 × 11	H400 × 200 × 8 × 13	H400 × 200 × 8 × 13	2	HSS 300 × 9
2	H400 × 200 × 8 × 13	H400 × 200 × 8 × 13	H390 × 200 × 10 × 16	1	HSS 300 × 9

3.1. Base excitations

The structure is subjected to the JR Takatori ground motion record. The amplitudes of the ground motion are gradually increased so that the 20%, 40%, 60%, and 100% of the ground motion is applied to the structure, respectively (Table 2). Then, the responses of ambient vibrations are recorded to determine the dynamic characteristics of the structure. The two horizontal components and the vertical component of the earthquake have been subjected to the structure simultaneously. Fig. 5 shows the acceleration time histories of these components. When 20% of the ground motion is applied, the structure behaves elastically with merely partial cracks occurring on the wall panels. It is to be noted that applying the 40% of the ground motion, which is proportional to the design earthquake, results in increasing the structural damage by reaching it to the yielding zone. When the structure is subjected to 60% of the earthquake, which is assumed to be equal to 1.5 times the design earthquake, significant damages, such as yielding at column bases and panel zones, and destruction in wall panels have occurred. Finally, under 100% of the earthquake, uniform distribution of the damage over the height of the structure shifts into a soft story mechanism, causing the structure to collapse. In this study, 60% of the unscaled ground motion is used for system identification and parameter estimation.

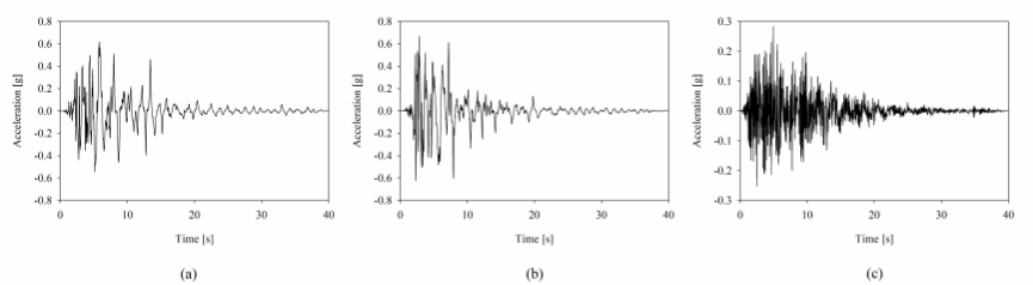

Fig. 5: Time histories of the unscaled JR Takatori motion components: (a) North-South component, (b) East-West component, and (c) vertical component.

Acceleration response spectrums of the three unscaled components of the JR Takatori ground motion are compared in Fig. 6. According to this figure, the horizontal components have significant spectral accelerations in the period range of 0 to 0.8 s, in the vicinity of the fundamental period of the structure in both east-west (EW) and north-south (NS) directions. However, the Y direction of the EW component is also stronger than that of the NS component. Thus, the structure is expected to experience more severe damages in the Y direction. In this study, to perform the 2D modeling of the structure, the frame of the Y-direction with no walls is used.

Table 2. Load sequence of earthquake excitations for the four-story test frame.

Load sequence	Excitation	Level
I	20% of the original JR Takatori record	Service level earthquake
II	40% of the original JR Takatori record	Design level earthquake
III	60% of the original JR Takatori record	Beyond design level earthquake
V	100% of the original JR Takatori record	Maximum considerable earthquake

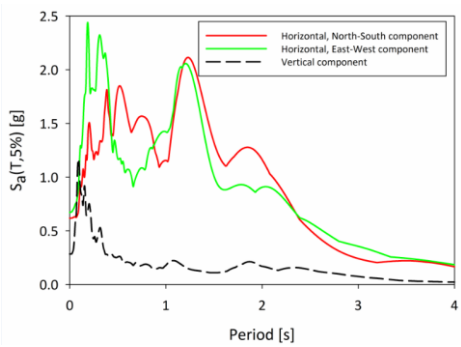

Fig. 6: Response spectrum of the two horizontal Y (North-South) and X (East-West), as well as the vertical components of the unscaled JR Takatori motion.

4. Finite element model

The finite element (FE) model of the frame is simulated in OpenSees platform [43]. In this study, two models, including 2D and 3D models, have been simulated to consider the uncertainties. In the 2D modeling, the concentrated plasticity is used to simulate the nonlinearity in beams, columns, and panel zones. Furthermore, panel zones are simulated by both parallelograms and scissors models. The frame with no wall panels has been modeled in the 2D model, in which the interaction of the frame and wall panels is not considered. The MIK material model is used to represent the inelastic behavior of beams and columns. Besides, the Krawinkler and Fielding and Huang models are used in the parallelogram and scissors methods, respectively (Fig. 7).

For the well-detailed 3D modeling, the beams and columns are simulated using the distributed plasticity and forced nonlinear beam-column elements. The G-M-P material model is assigned to fiber sections. The floor slabs are simulated using shell elements, and wall panels, which affect the lateral stiffness and strength of the structure (about 10% according to [44]), are modeled by the two methods shown in Fig. 7(d, e).To consider the interaction of wall panels and frames, three models including the frame with no wall panels, the frame with wall panels modeled by beam-column elements, and the frame with wall panel modeled by equivalent diagonal strut elements are employed. Among these models, the latter uses the concrete01 and general hysteretic material models for beam-column elements. Moreover, a slip model is used to simulate the diagonal elements of the walls. The details of the models are summarized in Table 3. The material models, modeling methodologies, and related unknown parameters are briefly discussed in the following sections.

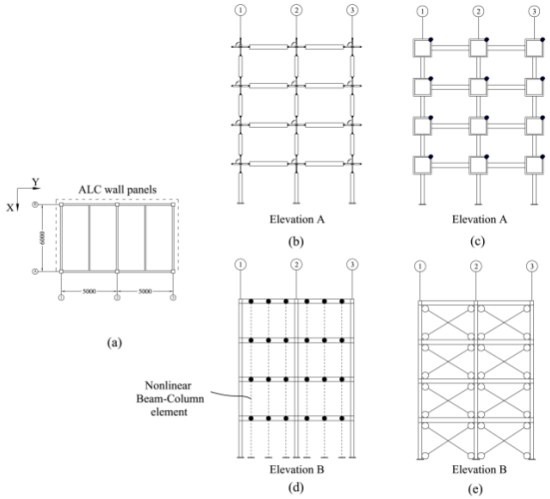

Fig. 7: Analytical model of the building prototype: (a) plan view of a typical story,(b) modeling of the panel zone region with the scissors methodology, (b) modeling of the panel zone region with the parallelogram methodology, (d) modeling of the wall panel with the beam-column element, and (e) modeling of the wall panel with the equivalent diagonal element.

Table 3. Properties and assumptions of the considered models.

		Plasticity Pattern for frame elements		Panel zone region		ALC Wall panel	
Model No.	Dim.	Methodology	Material	Methodology	Material	Methodology	Material
1	2-D	Concentrated	MIK				
2	2-D	Concentrated	MIK	Parallelogram	Krawinkler	-	-
3	3-D	Distributed	G-M-P	Scissors	Fielding and Huang	-	-
4	3-D	Distributed	G-M-P	-	-	Forced beam-column	Concrete01 +general hysteretic
5	3-D	Distributed	G-M-P	-	-	Equivalent diagonal strut	Slip based model

4.1. Modeling the nonlinear behavior of beams and columns using the concentrated plasticity

In this modeling, the regions with nonlinear behavior are simulated by the use of special elements. According to the mechanics of structures, since the nonlinearity under lateral seismic loads propagates in both depth and length of members, various uncertainties have existed in the modeling. For structural beams, in which axial loads are

negligible due to the rigid behavior of the floor slab diaphragm, the concentrated plasticity method can be advantageous. However, concerning the structural columns, the nonlinear behavior of columns is more complicated due to the presence of large axial loads. Consequently, lots of uncertainties have arisen in the modeling according to the concentrated plasticity method.

4.2. Modeling the nonlinear behavior of panel zones at the beam-to-column connections

For the moment-resisting steel connection, the high shear forces of the panel zone region located in the part of the column within the depth of the connecting beams cause nonlinear behavior in these components. Although the nonlinear behavior of well-designed panel zones may increase the energy dissipation capacity and provide a desirable hysteretic behavior, structural instability can arise. Since the panel zone is a susceptible region that may experience some level of distortion, the damage can be transferred to the connections. With regard to the experimental model of the structure, the rigid behavior of the floor slabs and its contribution to the flexural stiffness of the beams caused the beams to remain elastic under the seismic excitation of different levels. Besides, the nonlinear behavior was also observed in the panel zone regions. Hence, a thorough investigation of the behavior of panel zones is required.

Various methods of the panel zones' modeling in beam-column connections have been proposed in the literature, some of which are schematically illustrated in Fig. 8. The first method, known as the scissors method, is proposed by Castro et al. (Fig. 8(a)) [33]. In this method, two rigid elements connected by a nonlinear spring in the joint center, are used. The sizes of rigid elements equal to those of the connected beams and columns. Furthermore, the distortion occurs in each rigid element independently.

Biddah and Ghobarah [45] used three nonlinear springs to simulate the behavior of panel zones. Two springs simulate the rotation of the panel zone, while one spring simulates the shear force (Fig. 8(b)). Youssef and Ghobarah [46] utilized a parallelogram model whose corners are connected two by two, using translational springs to simulate the shear distortion. In this method, 12 springs are used to define different degradation patterns (Fig. 8(c)). Lowes and Altoontash [47] introduced a model with four nodes and 12 degrees of freedom to simulate the panel zone. In this method, a rotational spring and 12 translational springs were employed to display the shear force-distortion behavior as well as different degradation patterns in the panel zone (Fig. 8(d)). Krawinkler introduced a method that is known as the frame method in the literature [48]. According to this method, four rigid elements and a diagonal translational spring was used to model the behavior of the panel zone (Fig. 8(e)). Afterward, Krawinkler and Gupta introduced a method called the parallelogram method, which was similar to the previous method, except for a translational spring replaced with the rotational one. In this method, two nodes with the same coordinates in each corner and the same translational degrees of freedom were defined. Besides, the rotational spring in one of the corners displays the shear-distortion behavior [32] (Fig. 8(e)). Among various methods, some are too simplified like the scissors method, while others are too complicated, like the method proposed by Lowes and Altoontash. Simplified methods bring uncertainties to modeling. On the other hand, although complicated methods simulate the structure more accurately, a large number of unknown parameters make it difficult to identify the modeling of the structure. In this study, the scissors and parallelogram models were used.

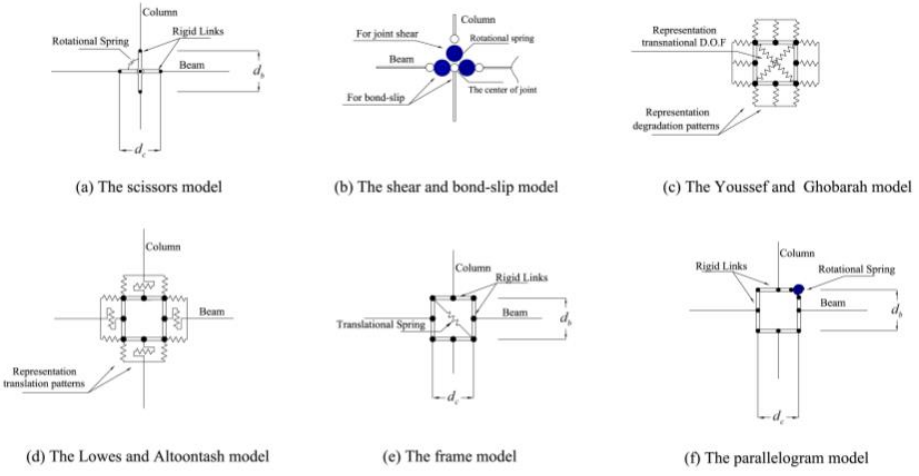

Fig. 8: Various modeling of the panel zone: (a) the scissors model, (b) the shear and bond-slip model, (c) the Youssef and Ghobarah model, (d) the Lowes and Altoontash model, (e) the frame model, and (f) the parallelogram model.

4.3. Modeling of panel walls

Precast panels, consisting of concrete materials are widely employed as infills and wall partitions in different structures, in which the elements, which play a significant role in the structural lateral stiffness and strength due to the interaction of the frame and its surrounding panels, are classified as nonstructural components of the structure. Hence, several damages to these components have been reported from past earthquakes. According to conducted research, the tested structure is surrounded by the ALC panels in all directions except for one of the Y-direction frames. The results demonstrate that the panels have experienced several damages through different levels of the earthquake [49]. As shown in Fig. 7(d,e), two main elements can be used for the modeling of panels: 1) an equivalent diagonal strut element in which two truss elements within the frame span are used, and 2) an equivalent beam-column element consisting of vertical elements. For the first method, material models and the effective width of the wall are the main parameters in determining the behavior of the wall. To examine the effective width of the wall, various methods have been proposed. In this study, the method proposed by Paulay and Priestley is utilized [50]. According to this method, the effective width of the wall is considered to be equal to ¼ of its length. For the second method, the model suggested by Tuan-Nam and Kasai is employed to demonstrate the force-displacement behavior of the wall [44].

In the second method, the walls are defined using fiber beam-column elements. As the width of the panels is almost 0.6 m, three panels are replaced by one beam-column element, located in the center of the panels. Additionally, the Concrete01 and general hysteretic material models of OpenSees have been applied for modeling the concrete and steel elements of the wall.

5. Material models

The prediction of the frame structures' behavior under an earthquake shaking requires accurate modeling that includes rules for the stiffness and strength deterioration. The Modified Ibarra–Krawinkler (MIK) deterioration model [34] is assigned to the idealized springs of beams and columns, and the *G-M-P* material model [37] is assigned to the fiber sections of beams and columns. The MIK model is based on a set of rules that define four cyclic deterioration patterns between the bounds. The Krawinkler and bi-linear mathematical models, introduced by Fielding and Huang, are assigned to the idealized springs of panel zones for the parallelogram and scissors methodologies, respectively. The shear-distortion responses of the mathematical models are described by tri-linear backbone curves.

5.1. MIK material model

The MIK material model was introduced by Ibarra et al. The model considers various degradations of the stiffness and strength, including yield strength degradation, post-yield stress degradation, reduction in loading, and unloading stiffness. As shown in Fig. 9(a,b), the parameters which are required to define the model are as follows: elastic stiffness, K_e; yield bending strength, M_y; capping strength, M_c; residual strength, M_r; yield curvature, θ_y; and some other parameters such as Λ, θ_p, θ_{pc} and θ_u. This model is used to describe the nonlinear behavior of beams and columns in the concentrated plasticity model.

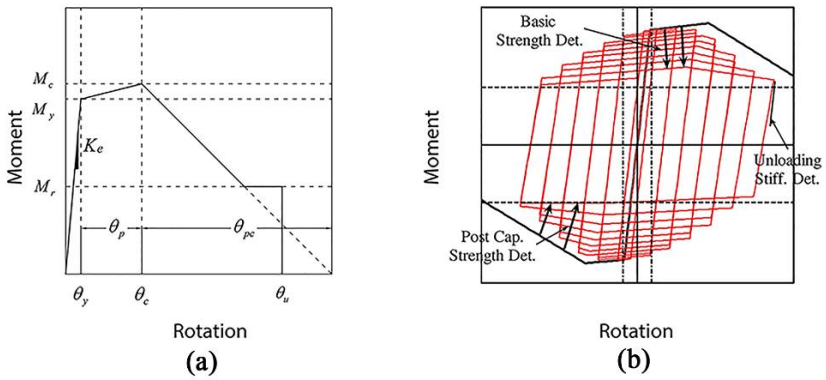

Fig. 9: Modified Ibara-Krawinkler deterioration model: (a) monotonic curve; (b) various modes of the cyclic deterioration (stiffness and strength deterioration) [51].

5.2. G-M-P material model

The G-M-P material model was proposed by [37]. The model formula consists of 8 parameters. As shown in Fig. 10(a), the parameters include the modulus of elasticity, E; yield stress, F_y; the ratio of post-yield hardening, b; and five other parameters, representing the effects of Bauschinger and isotropic hardening. For each substructure, the first three parameters are considered to be

unknown, while others can be defined based on the suggested values in the literature.

5.3. Concrete 01 model

The concrete 01 model was proposed by Karsan and Jirsa to describe concrete behavior [52]. According to Fig. 10(b), the sample is merely considered to have the compressive strength. Thus, the tensile strength is considered to be zero. The concrete01 model requires fewer parameters to be defined, including the maximum compressive stress, fpc, strain corresponding to the maximum compressive stress, $epsc0$, ultimate stress, $fpcu$, and strain corresponding to the ultimate stress, $epsu$, compared to other models.

5.4. *General hysteretic material model*

The general hysteretic model is a multilinear model in which the effects of pinching, cyclic degradation of the hysteretic energy, and reduction of unloading stiffness are considered. In this model, five parameters, including the PinchX, PinchY, damage1, damage2, and β, are needed in addition to the determined points on the backbone curve (Fig. 10(c)). PinchX and PinchY parameters are considered as the pinching of the stress and strain, respectively. Damage1 and damage2 parameters are defined as the damage caused by the ductility and energy dissipation, respectively, and β is defined as the degrading of unloading stiffness based on the ductility. In this study, only PinchX and PinchY parameters are considered as unknown parameters.

5.5. Slip-based material model

The Slip-based material model can be considered as a bilinear model, assigned to the equivalent diagonal elements which are used in the modeling of the walls [44]. As shown in Fig. 10(d), when the section strength reaches the maximum strength which corresponds to δ_1 displacement, the strength reduction at δ_2 displacement will be equal to zero. This model considers the separation and sliding between the infill and the frame. It is to be noted that the section strength, F and the parameters δ_1 and δ_2 are unknown.

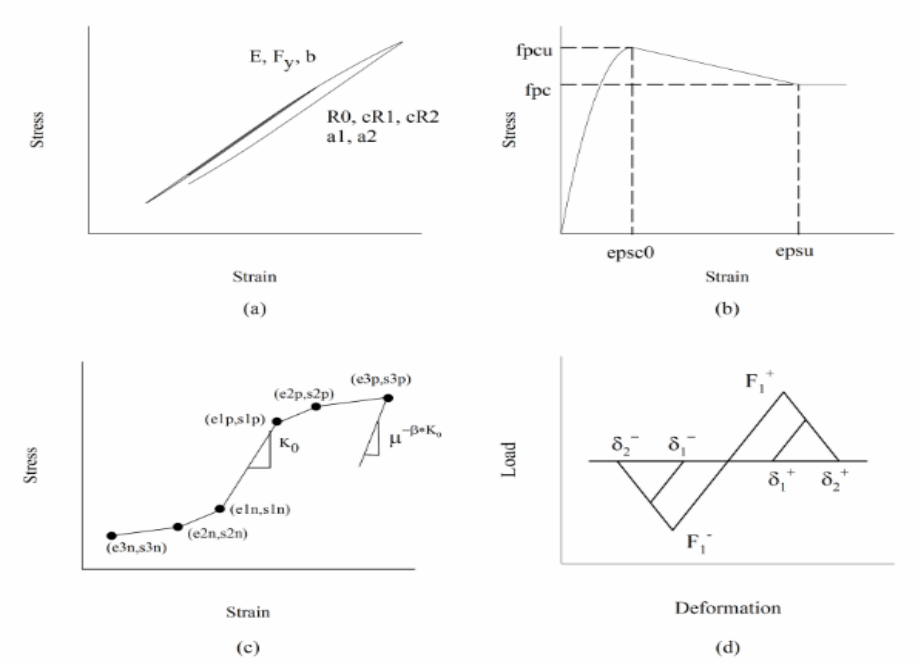

Fig. 10: Constitutive hysteretic principles considered for the modeling frame members and ALC wall panels: (a) G-M-P material model, (b) concrete01 material model, (c) general hysteretic material model, and (d) slip-based model.

5.6. Krawinkler material model

Several methods have been proposed to define the force-distortion relation of the panel zone region, one of which was introduced by Krawikler [35]. As illustrated in Fig. 11(a), the behavior of the trilinear curve is assigned to the rotational spring in the parallelogram model. In this model, the yield shear strength, V_y, is defined as:

$$V_y = \frac{F_y}{\sqrt{3}} A_v = \frac{F_y}{\sqrt{3}} (0.95 d_c t_{wc}) \approx 0.55 F_y d_c t_{cw} \qquad (21)$$

where d_c is the depth of the column section; t_{cw} is the web thickness, and F_y is the yield stress of the material. The strain corresponding to the section strength can be determined using the following equation:

$$\gamma_{y,1} = \frac{F_y}{\sqrt{3}\, G} \qquad (22)$$

Where G is the shear modulus of the column material.
The plastic strength of the column, V_p, is defined as:

$$V_p \approx 0.55F_y d_c t_{cw}(1+\frac{3b_{cf}t_{cf}^2}{d_b d_c t_{cw}}) \quad (23)$$

where t_{cf} and b_{cf} are the thickness and the width of the column flange respectively, and d_b is the depth of the beam section.
The elastic and post-yield stiffnesses denoted as K_e and K_p are obtained from the equations described below:

$$K_e = \frac{V_y}{\gamma_y} = 0.95 d_c t_{cw} G \quad (24)$$

$$K_p \approx 0.95G\frac{b_{cf}t_{cf}^2}{d_b} \quad (25)$$

According to this model, the distortion, $\gamma_{y,2}$, is considered to be equal to four times the $\gamma_{y,1}$

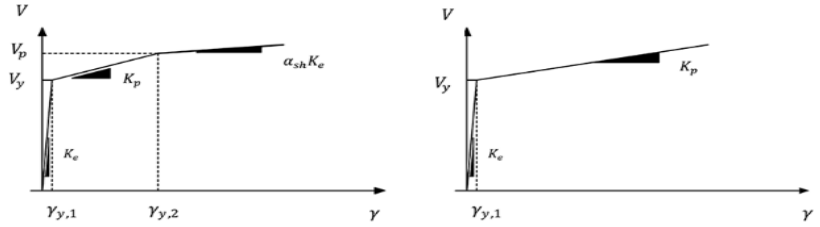

Fig. 11: Shear force-Distortion characteristics for the panel zone: (a) tri-linear mathematical model; (b) bilinear mathematical model.

5.7. Fielding and Huang material model

This model contains a bilinear curve, and the yield strength of the section is calculated by the following equation:

$$V_y = \frac{F_y}{\sqrt{3}}A_v = \frac{F_y}{\sqrt{3}}(d_c - t_{cf})t_{cw} \quad (26)$$

The post-yield stiffness is also defined as:

$$K_p = \frac{5.2Gb_{cf}\,b_{cf}^3}{d_b(1-\rho)} \quad (27)$$

In both material models used for the modeling of panel zone elements, the general hysteretic model is used. PinchX and PinchY parameters that have been mentioned above are also considered. The unknown parameters of five finite element models are classified in Table 4.

Table 4. Unknown considered material model parameters.

Model No.	Frame parameters	Panel zone region parameters	Wall panel parameters
1	$E,\ F_y\ ,\theta_p\ ,\ {M_c}/{M_y}\ ,\Lambda$	$E, F_y, PinchX, PinchY$	-
2	$E,\ F_y\ ,\theta_p\ ,\ {M_c}/{M_y}\ ,\Lambda$	$E, F_y, PinchX, PinchY$	-
3	$E,\ F_y\ , b$	-	-
4	$E,\ F_y\ , b$	-	$epsc0, epsu, fpc, fpcu$ $PinchX, PinchY$
5	$E,\ F_y\ , b$	-	F, δ_1, δ_2

6. Applications of PF and EKF algorithms in obtaining unknown model parameters

As mentioned previously, the PF and EKF methods are used to obtain the unknown parameters of the material models (Table 4). For this purpose, the finite element model is simulated in OpenSees framework. Then, the sensitivity matrix, the mean value, and the covariance matrix are computed, updated, and the errors are modified in MATLAB software [53]. In the PF method, the concept of the "range" is defined as the range of particle variations (material models parameters), according to Table 5. If the target values of parameters do not exist in this range, the system cannot be updated. Subsequently, the model may not be accurate enough to predict the unknown parameters. Hence, the selection of this range for the particles defined based on previous studies [41, 44, 51, 54], is of crucial importance. In the PF method, 500 particles are selected and modified during the time steps using the method of the aforementioned algorithm. In the EKF algorithm, initial values are assigned to the parameters as well as the covariance matrices, and mean values and covariance of the parameters are modified during the time steps. This process is iterated 100 times to obtain final values for parameters.
As mentioned earlier, the vectors v_k and η_k have normal probability distributions with the zero mean value and covariance matrices Q_k and R_K respectively. Along with the measurement of the responses of the structure, several

noises may be generated from different sources, including the sensor, sensor cable, and data acquisition system. Therefore, it is important to estimate the noises based on their source of generation. In this study, the Gaussian white noise with a zero mean value, and root mean square (RMS) noise-to-signal ratio (SNR) of 5% is assumed. Thus, the standard deviation of the noise is equal to $0.05 \times RMS\ (\ddot{y}_i)$ where $i = 1,2,3,4$ and $\ddot{y}$ is the acceleration of the first to fourth stories. Employing mentioned algorithm, parameters Q_k and R_k can be calculated [55]. Hence, the calculation of Q_k is implemented as follows:

Assuming that the second-order statistics of the process noise γ are time-invariant, the process noise covariance matrix is defined as $Q_k = Q = E(\gamma\gamma^T)$.

The covariance matrix is a diagonal matrix whose diagonal entries are the process noise variances associated with parameters to be estimated. Here, the variances are (as an example for model-1) considered as $(qF_{y0})^2$, $(qE_0)^2$, $(q\theta_{p0})^2$, $(q(M_c/M_y)_0)^2$, $(q\Lambda_0)^2$, $(qPinchX_0)^2$ and $(qPinchY_0)^2$, where $q = 10^{-4}$, that is, the RMS of each component of the process noise is taken 0.01% of the initial estimate of the corresponding material parameters [29, 56].

The covariance matrix R is considered as a diagonal matrix $= [R_{ii}]\ (i = 1, \dots)$, which means that the individual measurement noises are assumed to be statistically uncorrelated. The i[th] diagonal entry of R, R_{ii}, represents the variance of the individual measurement noise, v_i, corresponding to the i[th] measured response.

The amplitudes of the measurement noises are assumed to be unknown and considered as $RMS(v_i) = r \times RMS\ ([\ddot{y}_i])$, where $[\ddot{y}_i]$ denotes the time history of the i[th] measured response. The parameter $\ddot{y}_i$ is the noisy acceleration response of the i[th] floor. Thus, $R_{ii} = r^2 * (RMS[\ddot{y}_i])^2$ where r is considered 0.1 [29, 56].

With regard to several damage patterns and materials in the tested structure, different substructures have been defined. As such, the substructures are categorized as follows: 1) columns of the first story 2) panel zones of the first two stories in the 2D modeling 3) walls in the 3D modeling.

Table 5. The interval assumed for each constant parameter.

2-D modelling				3-D modelling			
Parameter	Columns of the first story	Parameter	Panel zones of the first two stories	Parameter	Columns of the first story	Parameter	Wall panel
$E(GPa)$	[160 240]	$E(GPa)$	[160 240]	$E(GPa)$	[160 240]	$epsc0$	[0.001 0.003]
$F_y(MPa)$	[240 360]	$F_y(MPa)$	[200 280]	$F_y(MPa)$	[240 360]	$epsu$	[0.006 0.012]
b	[0.005 0.015]	$PinchX$	[0.7 2]	b	[0.005 0.015]	$fpc(MPa)$	[8 18]
$\theta_p(rad)$	[0.02 0.05]	$PinchY$	[0.5 2]			$fpcu(MPa)$	[3 12]
M_c/M_y	[1.01 1.10]					$PinchX$	[0.5 1.5]
Λ	[0.5 2.0]					$PinchY$	[1 4]
						$F(KN)$	[10 40]
						$\delta_1(rad)$	[0.005 0.015]
						$\delta_2(rad)$	[0.015 0.025]

7. Results and discussion

Fig. 12 represents the parameters obtained from the PF algorithm for model_1. The parameters obtained from both PF and EKF methods are also compared in Table 6 for all models. According to this Table, the parameters possess different values in the two methods mentioned above. Although the differences are negligible for the modulus of elasticity values in columns and panel zones, considerable differences have been observed in the parameters related to walls. As can be seen, the more the parameters that affect the structural behavior, the fewer the uncertainties influencing the structural response, and vice versa.

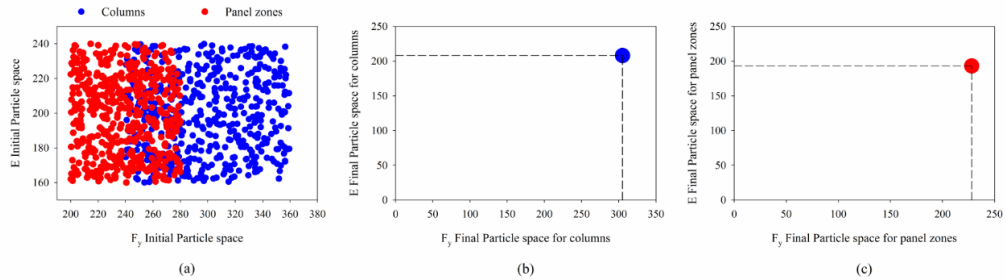

Fig. 12: Representation of the initial and final sample space of the Young module–yield stress parameter pairs for columns and panel zones for model_1: (a) initial sample space of the Young module –yield stress, (b) final sample space of the Young module –yield stress for columns, and (c) final sample space of the Young module –yield stress for panel zones.

Table 6. Comparision of the parameters obtained from PF to EKF algorithms.

Model No.	Algorithm	Columns					Panel zones			
		Parameters								
		$E(GPa)$	$F_y(MPa)$	θ_p	M_c/M_y	Λ	E	F_y	$PinchX$	$PinchY$
1	PF	208	305	0.027	1.08	1.8	193	228	1.3	0.7
	EKF	205	289	0.04	1.04	1.4	204	222	0.9	1.2
		Columns					Panel zones			
		Parameters								
2		E	F_y	θ_p	M_c/M_y	Λ	E	F_y	$PinchX$	$PinchY$
	PF	189	294	0.038	1.07	1.25	196	235	0.9	0.5
	EKF	193	301	0.032	1.09	0.95	200	247	1.25	1.0
		Parameters(columns)								
3		E	F_y	b						
	PF	198	276	0.0109						
	EKF	206	279	0.012						
		Columns			Wall panels					
		Parameters								
4		E	F_y	b	$epsc0$	$epsu$	fpc	$fpcu$	$PinchX$	$PinchY$
	PF	200	295	0.009	0.0012	0.01	12	5	0.5	2.5
	EKF	205	281	0.01	0.0015	0.011	11	6	0.75	3.5
		Columns			Wall panels					
		Parameters								
5		E	F_y	b	F	δ_1	δ_2			
	PF	202	285	0.008	24	0.01	0.016			
	EKF	198	284	0.007	15	0.013	0.02			

Fig. 13 represents the errors of story displacements in different models of the structure, examined under both PF and EKF methods. Among the 2D models for the panel zone, model_1 performed by the parallelogram method had fewer errors compared to model_2, performed by the scissors method. Additionally, this is the case for both PF and EKF algorithms. As can be seen, despite employing the PF algorithm, which includes a large number of particles and iterations, model_2 still had many uncertainties. On the other hand, panel zones significantly affected the nonlinear behavior of the structure so that using a method with less accuracy led to significant errors. Among the 3D models using the PF method, the model in which the walls are defined by beam-column elements (model_4) has the fewest errors. The most significant errors occurred in the model with the equivalent diagonal elements for the modeling of walls (model_5) and the model with no walls (model_3). In the EKF method, the results were dvaried to some extent. As can be noticed, despite the fewest errors of Model_5, no significant difference was observed, which implicitly shows that walls had fewer effects on the overall behavior of the structure, even after the cracking and damage caused by the base excitation. Moreover, the mechanical properties of material models used in walls have not been accurately determined. With regard to the structure with and without the effects of panel zone and wall in the 2D and 3D models, different behavior has been observed. As can be seen, although the PF method is more time-consuming than the EKF one, the difference between their calibrated models is not considerable.

Fig. 14 illustrates the curves for estimating the E and F_y for model_1(panel zones), ratio of post-yield hardening, b, for model_3 and δ_1 for model_5, in both PF and EKF methods. It is shown that E has changed from the beginning of the excitation and then became constant. While F_y changed when the structure entered the nonlinear zone. This is the case for both PF and EKF methods, but the values of their parameters are different from each other. In contrast, the estimations of the strain hardening ratio, b, start with a flat portion and then are followed by a rapidly changing portion. This portion begins after the structure becomes nonlinear, and its measured response is sufficiently sensitive to these parameters. Note that the post-yield parameters start updating later than the strength parameter F_y. δ_1 has changed from the beginning of the base excitation, which means early-stage damage occurred in walls.

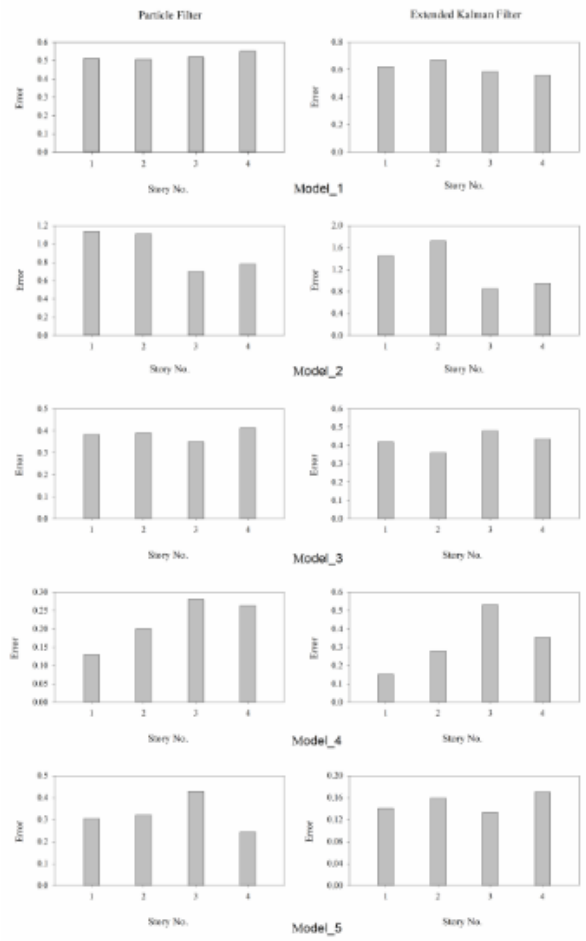

Fig. 13: Displacement error metrics for five calibrated four-story MRF models for the PF and EKF algorithms.

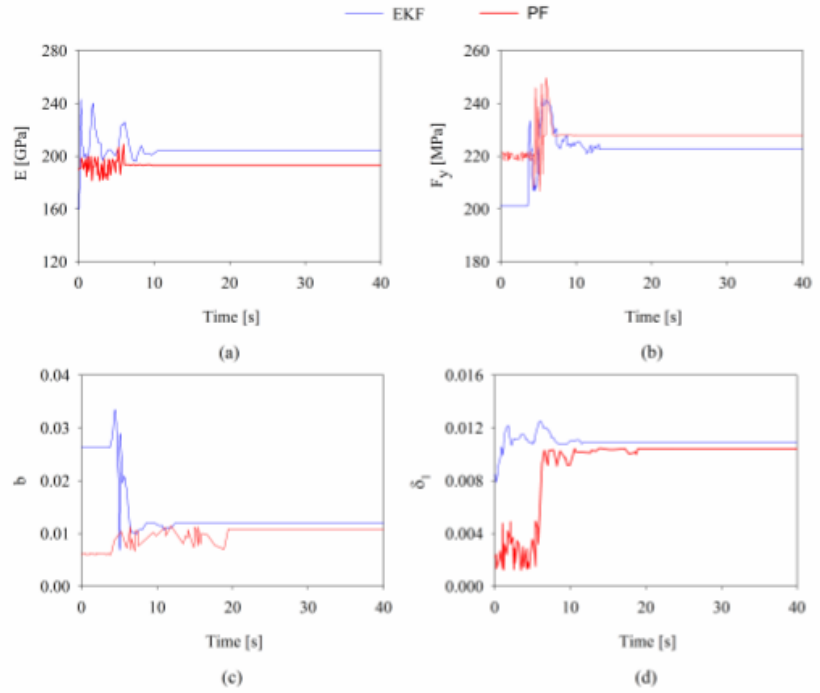

Fig. 14: Estimation of the results for the EKF and PF algorithms: (a) Young module for panel zone regions of model_1, (b) yield stress for panel zone regions of model_1, (c) the ratio of post-yield hardening, b, for the first story columns of model_3, and (d) δ_1 for the wall panels of model_5.

Conclusion

In this study, the effects of modeling uncertainties of a 4-story steel structure surrounded by walls, have been studied, using the two recursive PF and EKF methods. Different uncertainties, including the 2D and 3D modeling, concentrated or distributed plasticity methods, and two methods for the simulation of the panel zones and walls, have also been considered. The parameters of the material models assigned to the structural elements have been determined using the PF and EKF methods. In the EKF method, whose equations have been linearized in the state-space form, the results were more acceptable than those of the PF method in which a lot of particles (material model parameters) have been used for the structural calibration. Furthermore, the EKF method is less time-consuming. As such, the EKF has acceptable reliability to apply for the calibration of nonlinear systems. However, for systems with considerable nonlinearities, the EKF method may not be reliable enough and, therefore, further investigations would be imperative.

References

[1] Jaishi, B. and W.-X. Ren, *Structural finite element model updating using ambient vibration test results.* Journal of structural engineering, 2005. 131(4): p. 617-628.

[2] Marwala, T., *Finite element model updating using computational intelligence techniques: applications to structural dynamics*. 2010: Springer Science & Business Media.

[3] Friswell, M.I., J.E. Mottershead, and H. Ahmadian, *Finite–element model updating using experimental test data: parametrization and regularization.* Philosophical Transactions of the Royal Society of London. Series A: Mathematical, Physical and Engineering Sciences, 2001. 359(1778): p. 169-186.

[4] Jaishi, B. and W.-X. Ren, *Damage detection by finite element model updating using modal flexibility residual.* Journal of sound and vibration, 2006. 290(1-2): p. 369-387.

[5] Ren, W.-X. and H.-B. Chen, *Finite element model updating in structural dynamics by using the response surface method.* Engineering structures, 2010. 32(8): p. 2455-2465.

[6] Wu, J. and Q. Li, *Finite element model updating for a high-rise structure based on ambient vibration measurements.* Engineering Structures, 2004. 26(7): p. 979-990.

[7] Steenackers, G. and P. Guillaume, *Finite element model updating taking into account the uncertainty on the modal parameters estimates.* Journal of Sound and Vibration, 2006. 296(4-5): p. 919-934.

[8] Astroza, R. and A. Alessandri, *Effects of model uncertainty in nonlinear structural finite element model updating by numerical simulation of building structures.* Structural Control and Health Monitoring, 2019. 26(3): p. e2297.

[9] Bayraktar, A., B. Sevim, and A.C. Altunişik, *Finite element model updating effects on nonlinear seismic response of arch dam–reservoir–foundation systems.* Finite elements in analysis and design, 2011. 47(2): p. 85-97.

[10] Ebrahimian, H., et al., *Nonlinear finite element model updating for damage identification of civil structures using batch Bayesian estimation.* Mechanical Systems and Signal Processing, 2017. 84: p. 194-222.

[11] Asgarieh, E., B. Moaveni, and A. Stavridis, *Nonlinear finite element model updating of an infilled frame based on identified time-varying modal parameters during an earthquake.* Journal of Sound and Vibration, 2014. 333(23): p. 6057-6073.

[12] Ebrahimian, H., R. Astroza, and J.P. Conte, *Nonlinear Structural Finite Element Model Updating using Batch Bayesian Estimation*, in *Model Validation and Uncertainty Quantification, Volume 3*. 2015, Springer. p. 35-43.

[13] Astroza, R., A. Alessandri, and J.P. Conte, *A dual adaptive filtering approach for nonlinear finite element model updating accounting for modeling uncertainty.* Mechanical Systems and Signal Processing, 2019. 115: p. 782-800.

[14] Giagopoulos, D. and A. Arailopoulos, *Computational framework for model updating of large scale linear and nonlinear finite element models using state of the art evolution strategy.* Computers & Structures, 2017. 192: p. 210-232.

[15] Jategaonkar, R.V., *Flight vehicle system identification: A time-domain methodology*. 2015: American Institute of Aeronautics and Astronautics, Inc.

[16] Paleologu, C., J. Benesty, and S. Ciochina, *A robust variable forgetting factor recursive least-squares algorithm for system identification.* IEEE Signal Processing Letters, 2008. 15: p. 597-600.

[17] Ding, F., et al., *A recursive least squares parameter estimation algorithm for output nonlinear autoregressive systems using the input–output data filtering.* Journal of the Franklin Institute, 2017. 354(15): p. 6938-6955.

[18] Zhou, N., et al., *Robust RLS methods for online estimation of power system electromechanical modes.* IEEE Transactions on Power Systems, 2007. 22(3): p. 1240-1249.

[19] Andrieu, C., et al., *Particle methods for change detection, system identification, and control.* Proceedings of the IEEE, 2004. 92(3): p. 423-438.

[20] Schön, T.B., et al., *Sequential Monte Carlo methods for system identification.* IFAC-PapersOnLine, 2015. 48(28): p. 775-786.

[21] Chatzi, E.N. and A.W. Smyth, *The unscented Kalman filter and particle filter methods for nonlinear structural system identification with non-collocated heterogeneous sensing.* Structural Control and Health Monitoring: The Official Journal of the International Association for Structural Control and Monitoring and of the European Association for the Control of Structures, 2009. 16(1): p. 99-123.

[22] Azam, S.E. and S. Mariani, *Dual estimation of partially observed nonlinear structural systems: A particle filter approach.* Mechanics Research Communications, 2012. 46: p. 54-61.

[23] Chang, M. and S.N. Pakzad, *Observer Kalman filter identification for output-only systems using interactive structural modal identification toolsuite.* Journal of Bridge Engineering, 2014. 19(5): p. 04014002.

[24] Sato, T. and M. Sato, *Structural identification using neural network and Kalman filter algorithms.* Doboku Gakkai Ronbunshu, 1997. 1997(563): p. 1-10.

[25] Hoshiya, M. and A. Sutoh, *Kalman filter—finite element method in identification*. Journal of engineering mechanics, 1993. 119(2): p. 197-210.
[26] Lourens, E., et al., *An augmented Kalman filter for force identification in structural dynamics.* Mechanical Systems and Signal Processing, 2012. 27: p. 446-460.
[27] Jeen-Shang, L. and Z. Yigong, *Nonlinear structural identification using extended Kalman filter*. Computers & structures, 1994. 52(4): p. 757-764.
[28] Yang, J.N., et al., *An adaptive extended Kalman filter for structural damage identification.* Structural Control and Health Monitoring: The Official Journal of the International Association for Structural Control and Monitoring and of the European Association for the Control of Structures, 2006. 13(4): p. 849-867.
[29] Ebrahimian, H., R. Astroza, and J.P. Conte, *Extended Kalman filter for material parameter estimation in nonlinear structural finite element models using direct differentiation method.* Earthquake Engineering & Structural Dynamics, 2015. 44(10): p. 1495-1522.
[30] Hoshiya, M. and E. Saito, *Structural identification by extended Kalman filter.* Journal of engineering mechanics, 1984. 110(12): p. 1757-1770.
[31] Smyth, A., et al., *On-line parametric identification of MDOF nonlinear hysteretic systems.* Journal of Engineering Mechanics, 1999. 125(2): p. 133-142.
[32] Gupta, A. and H. Krawinkler, *Seismic demands for the performance evaluation of steel moment resisting frame structures*. 1998, Stanford University.
[33] Castro, J., A. Elghazouli, and B. Izzuddin, *Modelling of the panel zone in steel and composite moment frames.* Engineering structures, 2005. **27**(1): p. 129-144.
[34] Ibarra, L.F., R.A. Medina, and H. Krawinkler, *Hysteretic models that incorporate strength and stiffness deterioration.* Earthquake engineering & structural dynamics, 2005. 34(12): p. 1489-1511.
[35] Krawinkler, H., *Shear in beam-column joints in seismic design of steel frames.* Engineering Journal, 1978. 15(3).
[36] Fielding, D. and J. Huang, *Shear in steel beam-to-column connections.* Welding Journal, 1971. 50(7): p. 313-326.
[37] Filippou, F.C., V.V. Bertero, and E.P. Popov, *Effects of bond deterioration on hysteretic behavior of reinforced concrete joints.* 1983.
[38] Arulampalam, M.S., et al., *A tutorial on particle filters for online nonlinear/non-Gaussian Bayesian tracking.* IEEE Transactions on signal processing, 2002. 50(2): p. 174-188.
[39] Andrieu, C. and A. Doucet, *Particle filtering for partially observed Gaussian state space models.* Journal of the Royal Statistical Society: Series B (Statistical Methodology), 2002. 64(4): p. 827-836.
[40] Kwok, N.M., G. Fang, and W. Zhou. *Evolutionary particle filter: re-sampling from the genetic algorithm perspective*. in *2005 IEEE/RSJ International Conference on Intelligent Robots and Systems*. 2005. IEEE.
[41] Ebrahimian, H., R. Astroza, and J. Conte, *Parametric identification of hysteretic material constitutive laws in nonlinear finite element models using extended Kalman filter*. Department of Structural Engineering, University of California, San Diego, La Jolla, CA, 2014.
[42] Suita, K., et al. *Collapse experiment on 4-story steel moment frame: Part 2 detail of collapse behavior*. in *Proceedings of the 14th world conference on earthquake engineering, Beijing, China*. 2008.
[43] McKenna, F., *OpenSees: a framework for earthquake engineering simulation.* Computing in Science & Engineering, 2011. 13(4): p. 58-66.
[44] Tuan-Nam, T. and K. Kasai. *Study on Shaking-Table Experiment of a Full-Scale Four-Story Steel Building*. in *the 15th World Conference on Earthquake Engineering*. 2012.
[45] Biddah, A. and A. Ghobarah, *Modelling of shear deformation and bond slip in reinforced concrete joints.* Structural Engineering and Mechanics, 1999. **7**(4): p. 413-432.
[46] Youssef, M. and A. Ghobarah, *Modelling of RC beam-column joints and structural walls.* Journal of Earthquake Engineering, 2001. **5**(01): p. 93-111.
[47] Lowes, L.N. and A. Altoontash, *Modeling reinforced-concrete beam-column joints subjected to cyclic loading.* Journal of Structural Engineering, 2003. 129(12): p. 1686-1697.
[48] Krawinkler, H., *Inelastic behavior of steel beam-to-column subassemblages*. Vol. 71. 1971: University of California, Berkeley.
[49] Matsuoka, Y., et al. *Non-structural component performance in 4-story frame tested to collapse*. in *Proceedings of the 14th World Conference on Earthquake Engineering*. 2008.
[50] Paulay, T. and M.N. Priestley, *Seismic design of reinforced concrete and masonry buildings.* 1992.
[51] Lignos, D., H. Krawinkler, and A. Whittaker, *Prediction and validation of sidesway collapse of two scale models of a 4-story steel moment frame.* Earthquake Engineering & Structural Dynamics, 2011. 40(7): p. 807-825.
[52] Karsan, I.D. and J.O. Jirsa, *Behavior of concrete under compressive loadings.* Journal of the Structural Division, 1969.
[53] Grant, M., S. Boyd, and Y. Ye, *CVX: Matlab software for disciplined convex programming*. 2009.
[54] Gokmen, F., et al., *In situ seismic testing of a reinforced autoclaved aerated concrete building.* ce/papers, 2018. 2(4): p. 253-258.
[55] Koh, C. and L. See, *Identification and uncertainty estimation of structural parameters.* Journal of Engineering Mechanics, 1994. 120(6): p. 1219-1236.
[56] Astroza, R., H. Ebrahimian, and J.P. Conte, *Material parameter identification in distributed plasticity FE models of frame-type structures using nonlinear stochastic filtering.* Journal of Engineering Mechanics, 2015. 141(5): p. 04014149.